International Journal of Nanomedicine

Dovepress
open access to scientific and medical research

Open Access Full Text Article

ORIGINAL RESEARCH

Folate Decorated Multifunctional Biodegradable Nanoparticles for Gastric Carcinoma Active Targeting Theranostics

Xin Zhang[1,*], Ronglin Yan[1,*], Ziran Wei[1,*], Dejun Yang[1], Zunqi Hu[1], Yu Zhang[1], Xin Huang[1], Hejing Huang[2], Weijun Wang[1]

[1]Department of Gastrointestinal Surgery, Second Affiliated Hospital of Naval Medical University, Shanghai, 200003, People's Republic of China; [2]Department of Ultrasound, Second Affiliated Hospital of Naval Medical University, Shanghai, 200003, People's Republic of China

*These authors contributed equally to this work

Correspondence: Hejing Huang, Tel +86-21-81886051, Email huanghejinga@163.com; Weijun Wang, Tel +86-21-81885602, Email wangweijun@smmu.edu.cn

Introduction: Gastric cancer remains a major clinical issue and little progress has been made in the treatment of gastric cancer patients during recent decades. Nanoparticles provide a versatile platform for the diagnosis and treatment of gastric cancer.

Methods: We prepared 7-ethyl-10-hydroxycamptothecin (SN-38) ^{125}I-radiolabelled biodegradable nanoparticles with folate surface modification (^{125}I-SN-38-FA-NPs) as a novel nanoplatform for targeted gastric carcinoma theranostics. We characterized this system in terms of particle size, morphology, radiostability, and release properties and examined the in vitro cytotoxicity and cellular uptake properties of ^{125}I-SN-38-FA-NPs in MNK 7 and NCI-N7 cells. The pharmacokinetics and biodistribution of ^{125}I-SN-38-FA-NPs were imaged by single photon emission computer tomography (SPECT). An MNK7 tumor-bearing model were established and the in vivo antitumor activity of ^{125}I-SN-38-FA-NPs was evaluated.

Results: SN-38 was readily radiolabeled with ^{125}I and exhibited high radiostability. Poly-lactic-co-glycolic acid (PLGA) nanoparticles (NPs) were formed by solvent exchange, and displayed spherical morphology of 100 nm in diameter as characterized by dynamic light scattering (DLS) and transmission electron microscopy (TEM). A 2.5-fold greater uptake of ^{125}I-radiolabelled SN-38-loaded folate-decorated PLGA nanoparticles (^{125}I-SN-38-FA-NPs) than ^{125}I-radiolabelled SN-38-loaded PLGA nanoparticles (^{125}I-SN-38-NPs) were record in MKN7 tumor cells. NPs and folate-decorated PLGA nanoparticles (FA-NPs) also had good biocompatibility in methyl thiazolyl tetrazolium (MTT) assays. Pharmacokinetic, biodistribution and SPECT imaging studies showed that ^{125}I-SN-38-FA-NPs had prolonged circulation, were distributed in the reticuloendothelial system, and had high uptake in tumors with a higher tumor accumulation of ^{125}I-SN-38-FA-NPs than ^{125}I-SN-38-NPs recorded at 24 h postinjection. In vivo SN-38-FA-NPs significantly inhibited tumor growth without causing obvious side effects.

Conclusion: Folate receptor alpha (FOLR1) targeted drug-loaded nanoparticles enable SPECT imaging and chemotherapy, and provide a novel nanoplatform for gastric carcinoma active targeting theranostics.

Keywords: folate, biodegradable nanoparticles, active targeting, SN-38, SPECT

Introduction

Gastric carcinoma is a malignant tumor originating from the epithelium of the gastric mucosa. It is a global health issue, with more than one million cases newly diagnosed worldwide each year. However, there have not been any significant advances in treatment.[1,2] Chemotherapy remains one of the most commonly used strategies for the treatment of gastric cancer in clinical practice.[3,4] Camptothecin chemotherapeutics, such as 7-ethyl-10-hydroxycamptothecin (SN-38), have attracted much attention because they can inhibit DNA replication by inhibiting topoisomerase activity.[5,6] However, the highly nonpolar nature of SN-38 leading to poor solubility in aqueous solution and hydrolysis of the lactone ring at pH>6 to creat an inactive carboxylate form, limits its clinical use. Moreover, the side effects accompanying effective doses, such as

Received: 8 November 2021
Accepted: 24 May 2022
Published: 31 May 2022

myelosuppression, diarrhoea and heamatemesis, further restrict the application of SN-38.[7–9] Over recent decades, to address the limitations of chemotherapeutics drugs, nanocarriers-especially polymeric nanoparticle delivery systems, with superior aqueous dispersity and biocompatibility, have been explored for use in cancer treatment.[10–12] Polymeric nanoparticles are stable and easy to fabricate because they: have tunable properties; are biocompatible and easy to translate clinically; have been studied in preclinical and clinical settings in recent decades. Some polymers, such as poly-lactic-co-glycolic acid (PLGA), have been approved by the Food Drug Administration (FDA).[13,14] Unlike small-molecule chemotherapeutics, nanoparticles have a long blood circulation time and are preferentially accumulated in tumors (with limited distribution in healthy tissue), making them ideal for cancer treatment.[15–17]

Although some studies have reported a small, or negative, effects with targeted ligand modification, many have shown it increases the tumor accumulation of nanoparticles, including those containing folate, that can bind to the folate receptor. The folate receptor is a glycosylphosphatidylinositol-linked protein frequently overexpressed in many tumors, such as gastric carcinoma, ovarian and breast cancer.[18–20] Folate-modified nanoparticles display efficient targeting ability in tumor diagnosis and treatment[21–24] for instance, a folate-targeted polymeric nanoparticle formulation of docetaxel is an effective molecularly targeted radiosensitizer for head and neck cancer.[25]

Nuclear imaging, such as single photon emission computer tomography (SPECT) or positron emission tomography (PET), is a noninvasive imaging modality that quantifiably detects infinitely penetrating gamma rays emitted by radionuclides, providing functional information suitable for preclinical study and clinical diagnosis.[26–28] For example, Sirianni et al reported the use of ^{18}F radiolabelled PLGA nanoparticles for brain imaging.[29] In recent decades, approaches combining imaging and therapy, called theranostics, have attracted tremendous attention as a future strategy for personalized medicine.[26] Due to the many advantages of nanoparticles, they can offer a platform for both diagnosis and therapy.[30,31]

We designed folate-modified biodegradable nanoparticles loaded with SN-38 for the actively targeted gastric carcinoma. SN-38-loaded nanoparticles radiolabelled with radioiodine (^{125}I) were developed as diagnostic agents for SPECT imaging to quantify their biodistribution and accumulation in tumors. Folate was used as a targeting ligand to actively target folate receptor-overexpressing tumor cells. SN-38 was controllably released from folate-modified biodegradable nanoparticles to allow targeting of gastric cancer cells.

Materials and Methods

Preparation and Characterization of Nanoparticles

PLGA nanoparticles (NPs) were prepared by precipitation.[32] Nanoparticles were used to encapsulate the hydrophobic drug SN-38 within the hydrophobic core by phase separation. DSPE-PEG (6 mg) and PLGA (4 mg) were dissolved in 100 μL chloroform and 100 μL dimethyl sulfoxide (DMSO) and the chloroform allowed to evaporate. The polymer-DMSO solution was added to deionized water and stirred, before removal of the DMSO by ultracentrifugation at 3000 rpm. The concentration of NPs was fixed at 10 mg/mL by controlling the volume of solvent using ultrafiltration. To prepare folate-decorated PLGA nanoparticles (FA-NPs), a similar method was used: DSPE-PEG (4.8 mg), DSPE-PEG-FA (1.2 mg), and PLGA (4 mg) were dissolved in 100 μL chloroform and 100 μL DMSO. SN-38-loaded folate-decorated PLGA nanoparticles (SN-38-FA-NPs) were prepared with DSPE-PEG (4.8 mg), DSPE-PEG-FA (1.2 mg), PLGA (4 mg) and SN-38 (1 mg) by the same method.

The hydrodynamic diameter of the NPs was measured by dynamic light scattering (DLS) at 25 °C on a Malvern Zetasizer Nano ZS90 equipped with a solid-state He−Ne laser (λ = 633 nm), and the measurements were repeated in triplicate. The stability of the NPs was measured by DLS on Days 1, 2, 3, 5 and 7 under the same conditions. The morphology of the NPs was characterized by transmission electron microscopy (TEM) (Tecnai F20, FEI, Japan) at 120 keV voltage. The NPs were applied to a carbon-coated copper grid and incubated for 15 min with excess solution removed by filter paper. An aqueous solution of phosphotungstic acid (10 mg/mL, 10 μL) was then applied to the copper grid for 3 min to dye the nanoparticles.

^{125}I-radiolabelled SN-38 (^{125}I-SN-38) was prepared by the iodogen method.[33] SN-38 was dissolved in DMSO and added to an iodogen tube with NaI (^{125}I) (1 mCi) for 30 min. The radiolabelling efficiency was determined by thin layer

chromatography (TLC) using HCl (pH=3) solution as a mobile phase. The radioactivity of ^{125}I was measured by a gamma counter (Multi Crystal LB2111, Germany). A retention factor (R_f) of ^{125}I-SN-38 ~ 0.1, and of free ^{125}I ~ 0.9 were obtained by TLC.

The encapsulation efficiency (*EE%*) and drug loading efficiency (*DL%*) of SN-38 were determined by using ^{125}I-SN-38 to prepare ^{125}I-radiolabelled SN-38-loaded PLGA nanoparticles (^{125}I-SN-38-NPs). The encapsulation efficiency (*EE* %) and drug loading efficiency (*DL*%) were calculated according to the following equation:

$$EE\% = \frac{R_2}{R_1 + R_2} \text{x} 100\%$$

$$DL\% = \frac{\text{EE\% x } w_1}{w_1 + w_2} \text{x} 100\%$$

R_1 and R_2 refer to the radioactivity of unencapsulated and encapsulated ^{125}I-SN-38, and w_1 and w_2 refer to the mass of ^{125}I-SN-38 and NPs.

The cumulative release of SN-38 was assessed by measuring the radioactivity of ^{125}I-SN-38 at pH 5 and 7.4 over time by dialysis against PBS. The ^{125}I-SN-38-NPs solution was incubated at 37 °C, and the radioactivity was measured at 1, 2, 4, 24, 48, 72, 96, 120, and 144 h.

Cellular Uptake and Cytotoxicity of Nanoparticles in Human Gastric Cancer Cell Lines

The human gastric cancer cell lines MKN7 and NCI-N87 were purchased from the Center for Excellence in Molecular Cell Science (CAS). Cells were cultured in DMEM supplemented with 10% fetal bovine serum (FBS) at 37 °C for 24 h in a 5% CO_2 atmosphere. Concentrations of 35, 70, 140, 280, and 560 μg/mL nanoparticles of ^{125}I-SN-38-NPs and ^{125}I-radiolabelled SN-38-loaded folate-decorated PLGA nanoparticles (^{125}I-SN-38-FA-NPs) respectively, were added to the cells and incubated for 2 h. Media was removed by centrifugation, the cells washed three times with PBS, and the radioactivity measured using a gamma counter.

Methyl thiazolyl tetrazolium (MTT) assays were used to evaluate the cytotoxicity of NPs, FA-NPs, SN-38 loaded PLGA nanoparticles (SN-38-NPs) and SN-38-loaded folate-decorated PLGA nanoparticles (SN-38-FA-NPs). MKN7 cells were seeded and cultured in a 96-well plate (1×10^4 cells/well) in DMEM with 10% FBS at 37 °C for 24 h in a 5% CO_2 atmosphere. Medium was aspirated and replaced by NPs, FA-NPs, SN-38-NPs, and SN-38-FA-NPs, each at a range of concentrations (0, 12.5, 25, 50, and 100 μg/mL nanoparticles) respectively, and incubated at 37 °C for 24 h. Cells were then cultured with 3-(4,5-dimethylthiazol-2-yl)-2,5-diphenyltetrazolium bromide solution (100 μL, 0.5 mg/mL) for 4 h before the addition of DMSO (100 μL). A microplate reader (Thermo, Varioskan Flash) was used to measure the absorption of each solution at 490 nm.

Pharmacokinetics and Biodistribution of Nanoparticles in Tumor-Bearing Mice

Female BALB/c mice (6 weeks old, each weighing 18–20 g) of specific pathogen-free (SPF) grade were purchased from the Shanghai SLAC Laboratory Animal Co., Ltd. To investigate the pharmacokinetics, ^{125}I-SN-38-NPs (100 mg/kg nanoparticles, 20 μCi) and ^{125}I-SN-38-FA-NPs (100 mg/kg nanoparticles, 20 μCi) were intravenously injected into healthy mice via the tail vein. Blood was obtained from the mouse retro-orbitally over time, weighed, and the radioactivity was measured using a gamma counter.

To establish a gastric tumor model, MKN7 cells (5×10^6) were injected into the right hind leg of nude BALB/c mice (6 weeks old, each weighing 20–25 g). Antitumor efficiency study was performed when tumor volume reached approximately 100 mm^3, and biodistribution and imaging studies were performed when tumor volume reached approximately 200–250 mm^3. To investigate the biodistribution, MKN7 tumor-bearing nude BALB/c mice were intravenously injected with ^{125}I-SN-38-NPs (100 mg/kg nanoparticles, 20 μCi) and ^{125}I-SN-38-FA-NPs (100 mg/kg nanoparticles, 20 μCi). At 24 h postinjection the mice were sacrificed, and the major organs (heart, lung, liver, spleen, and kidney), and tumors,

were harvested. The weights of the organs and tumors were determined and the radioactivity of each was measured using a gamma counter.

For the imaging study, *micro*SPECT scans were performed on MKN7 tumor-bearing mice after intravenous injection with ^{125}I-SN-38-NPs (100 mg/kg nanoparticles, 200 μCi) and ^{125}I-SN-38-FA-NPs (100 mg/kg nanoparticles, 200 μCi). The *micro*SPECT/CT was scanned at 0.5, 3, 6, 9, and 24 h with the *micro*SPECT scan set at 15 min and the CT scan at 55 keV tube voltage and 615 mA tube current.

In vivo Therapy Using Nanoparticles in Tumor-Bearing Mice

MKN7 subcutaneous tumor-bearing mice (~100 mm^3) were randomly divided into 5 treatment groups: PBS, NPs, FA-NPs, SN-38-NPs, and SN-38-FA-NPs (100 mg/kg nanoparticles). PBS and NPs were administered via the tail vein on Days 0, 5, 10, 15, and 20, with 20 days of recovery. Mouse weight was measured with a balance every 5 days. Tumor volume was measured with a Vernier caliper and calculated using the following equation:

$$V = \frac{L \mathrm{x} W \mathrm{x} W}{2}$$

L and *W* correspond to the length and width of the tumor, respectively. On Day 21, one of the mice in each group was sacrificed. Major organs and tumors were sliced for haematoxylin and eosin (H&E) and TUNEL staining.[34,35] After staining, the slices were observed by optical microscopy (Olympus IX73) and laser scanning confocal microscopy (Olympus FV1200).

Results and Discussion

Preparation and Characterization of Nanoparticles

SN-38-FA-NPs were prepared using solvent exchange by dissolving DSPE-PEG, DSPE-PEG-FA, SN-38, and PLGA in DMSO and mixing with deionized water. Nanoparticles were obtained by removing DMSO after ultracentrifugation. NPs, FA-NPs, and SN-38-NPs were prepared using the same method. DLS showed that the hydrodynamic sizes of the NPs, FA-NPs, SN-38-NPs, and SN-38-FA-NPs were about 100 nm, with a narrow size distribution (PDI<0.2). TEM confirmed that the morphology of the NPs was spherical, with a size of approximately 100 nm (Figure 1A). To evaluate the colloidal stability of NPs, the hydrodynamic size was measured by DLS at room temperature over time. It was found that the hydrodynamic size of NPs in PBS stayed significantly constant for up to one week, indicating colloidal stability (Figure 1B).

To quantitatively investigate the biodistribution of SN-38, ^{125}I-SN-38 was radiolabelled by a redox method using iodogen as an oxidant. The radiolabelling efficiency was determined by TLC, using HCl (pH=3) as a mobile phase. The radiolabeling efficiency was 69.2±1.5%, attributable to replacement of the active hydrogen located beside the phenolic hydroxyl group of SN-38 with radioiodine.[36,37] The radiostability of ^{125}I-SN-38 was examined in 10% FBS at 37 °C over time by TLC (Figure S1). Less than 2% free radioiodine (^{125}I) was found in solution at 96 h, indicating ^{125}I-SN-38 had the required radiostability to enable in vivo study (Figure 1C).

To characterize the encapsulation and loading efficiency of SN-38, ^{125}I-SN-38 was loaded into the nanoparticles, and the radioactivity of ^{125}I-SN-38 was measured by a gamma counter. The encapsulation efficiency was 93.3 ± 1.3%, while the loading efficiency was 8.5 ± 0.1%. The high SN-38 encapsulation efficiency may be due to the strong hydrophobicity of SN-38 at low pH.[38] Moreover, the cumulative release of SN-38 was characterized by dialysis against PBS at pH 5 and 7.4 at 37 °C by measuring the radioactivity of ^{125}I-SN-38 over time. ^{125}I-SN-38 was rapidly released, and 85.9 ± 1.8% of ^{125}I-SN-38 was present in solution after 144 h at pH 5 (Figure 1D). PLGA is known to accelerate degradation in a low pH environment.[39,40]

Affinity and Cytotoxicity of Nanoparticles

Targeted molecular modification of nanoparticle surfaces is a common strategy used to enhance the accumulation of nanoparticles on tumor and improve treatment. It has been reported that MKN7 cells overexpress folate receptors.[41] To investigate the targeting capability of folate-modified nanoparticles, we tested the affinity of ^{125}I-SN-38-FA-NPs by measuring the radioactivity of ^{125}I-SN-38 incubated with MKN7 cells at 37 °C for 1 h. The cellular uptake of ^{125}I-SN-38-

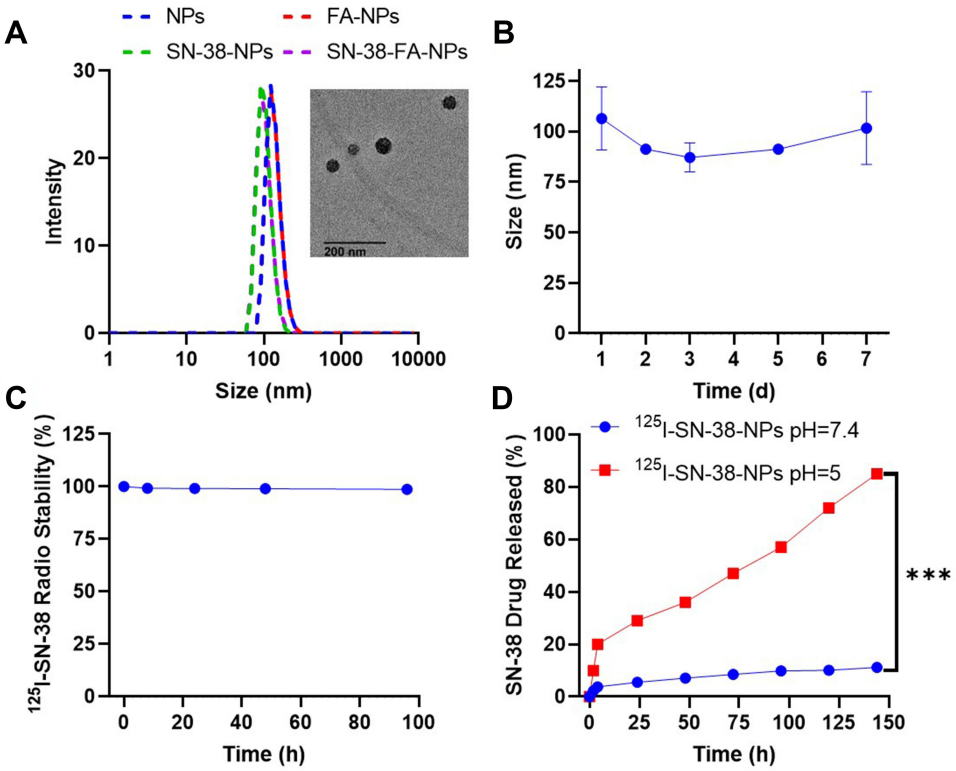

Figure 1 Characterization of nanoparticles. (**A**) The hydrodynamic size and morphology of nanoparticles were characterized by DLS and TEM. (**B**) Colloidal stability of NPs was measured by DLS. (**C**) Radiostability of ^{125}I-SN-38 was measured by TLC in 10% FBS at 37 °C. (**D**) Cumulative release of ^{125}I-SN-38 at pH 5 and 7.4 at 37 °C over time. ***p < 0.001 were considered highly significant.

FA-NPs was higher than that of ^{125}I-SN-38-NPs, particularly at high concentrations. The uptake of ^{125}I-SN-38-FA-NPs was 2.5 times high than that of ^{125}I-SN-38-NPs in MKN7 cells at a nanoparticle concentration of 560 mg/mL. The affinity of ^{125}I-SN-38-FA-NPs in NCI-N87 cell lines with low folate receptor expression, was also tested. The uptake of ^{125}I-SN-38-FA-NPs in NCI-N87 cells was low and comparable to the uptake of ^{125}I-SN-38-NPs in MKN7 cells, indicating that FA can enhance the uptake of nanoparticles in MKN7 cells (Figure 2A).

Prior to the in vivo study, we tested the cytotoxicity of SN-38-FA-NPs by MTT assays in MKN7 cells. The results showed no obvious cytotoxicity even with NPs at a concentration of 100 μg/mL, confirming previous reports that PLGA-based hybrid nanocarriers display a high level of biocompatibility.[42,43] It was found that the viability of MKN7 cells decreased with

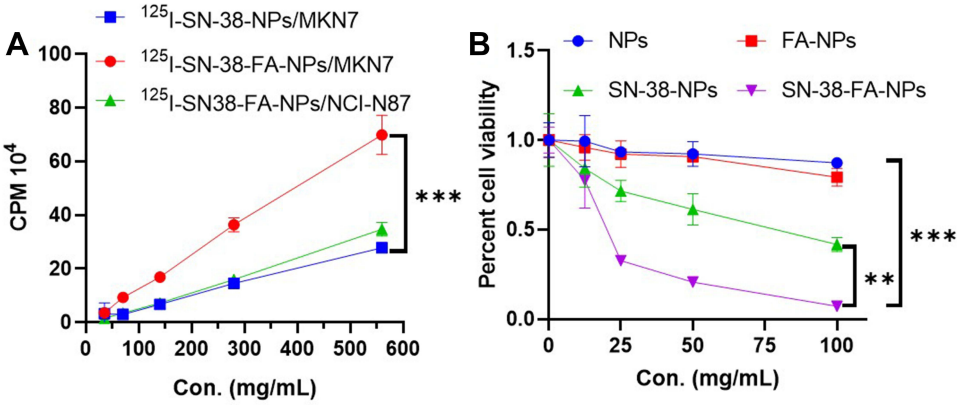

Figure 2 (**A**) Cell uptake of ^{125}I-SN-38-NPs and ^{125}I-SN-38-FA-NPs in MKN7 cells and ^{125}I-SN-38-FA-NPs in NCI-N87 cells at concentrations varying from 35 to 560 μg/mL after 2 h incubation. (**B**) MTT assay of nanoparticles with concentrations varying from 12.5 to 100 μg/mL at 37 °C after 24 h incubation. **p < 0.01 and ***p < 0.001 were considered highly significant.

increasing concentrations of SN-38-NPs and SN-38-FA-NPs. The half maximal inhibitory concentrations (IC50) of SN-38-NPs and SN-38-FA-NPs were 66.5 μmol/L and 14.0 μmol/L, respectively, determined by fitting the dose curve with cell viability (Figure 2B). The cytotoxicity results demonstrate that NPs and FA-NPs have good biocompatibility, and that SN-38-NPs and SN-38-FA-NPs can effectively inhibit the growth of MKN7 cells, perhaps attributable to PLGA degradation in the mid- to late endosomes (pH = 4.5–5.5) of cancer cells and the release of SN-38.[39,40]

Pharmacokinetics and Biodistribution of Nanoparticles

Pharmacokinetic studies of ^{125}I-SN-38-FA-NPs were carried out using healthy nude BALB/c mice by intravenous injection via the tail vein. Blood was collected from the retinal vein and weighed at different postinjection times, the radioactivity of ^{125}I-SN-38-FA-NP was measured using a gamma counter. The percentage injection dose per gram of blood varied over time (Figure 3A). The blood circulation of nanoparticles follows a two-compartment model.[44] In accordance with the model, ^{125}I-SN-38-NPs and ^{125}I-SN-38-FA-NPs displayed long blood circulation times with distribution half-lives of 0.22 h and 0.14 h, respectively. The elimination half-lives of ^{125}I-SN-38-NPs and ^{125}I-SN-38-FA-NPs were 6.6 h and 5 h, respectively. Generally, targeting ligand modifications reduced the circulation time, which is consistent with previous studies.[45] It has been reported that SN-38 is quickly replaced by SN-38 glucuronide and an unknown metabolite (M-2) after dosing in rats, and that the half-life of unchanged SN-38 is only approximately 7 min.[46] Our results demonstrate that ^{125}I-SN-38-NPs and ^{125}I-SN-38-FA-NPs exhibit significantly prolonged blood circulation and less hydrolysis of SN-38 than is achieved through direct administration of SN-38.

The biodistribution of ^{125}I-SN-38-FA-NPs was also determined in MKN7 tumor-bearing nude BALB/c mice after intravenous injection through the tail vein. At 24 h post-injection, the mice were sacrificed, the major organs and tumors were weighed, and the radioactivity of each tissue was measured. The accumulation of ^{125}I-SN-38-FA-NPs in tumors was 9.2 ± 0.6% ID/g, which was higher than that of ^{125}I-SN-38-NPs (3.3 ± 0.6% ID/g), indicating that FA-decorated nanoparticles have better tumor targeting ability. Nanoparticles can accumulate in tumors through enhanced permeation and retention (EPR) effect or nanomaterial-induced endothelial leakiness, while targeted modification can enhance accumulation within tumors.[47,48] The biodistribution of ^{125}I-SN-38-FA-NPs and ^{125}I-SN-38-NPs in the major organs was quantified over time from SPECT images (Figure S2). The accumulation of ^{125}I-SN-38-FA-NPs was high in the liver (28.2 ± 1.4%ID/g) and spleen (25.5 ± 3.2%ID/g), and was consistent with the behavior of other nanoparticles (Figure 3B). It is proposed that the biodistribution of nanoparticles was high in the liver and spleen due to uptake by the mononuclear phagocyte system.

The tumor accumulation of ^{125}I-SN-38-FA-NPs in MKN7 tumor-bearing mice was studied by *micro*SPECT following intravenous injection. Nuclear imaging provides a method for noninvasive diagnosis and accurate quantification of tumors. SPECT images showed the radioactive ^{125}I signal corresponded to the distribution of ^{125}I-SN-38-FA-NPs

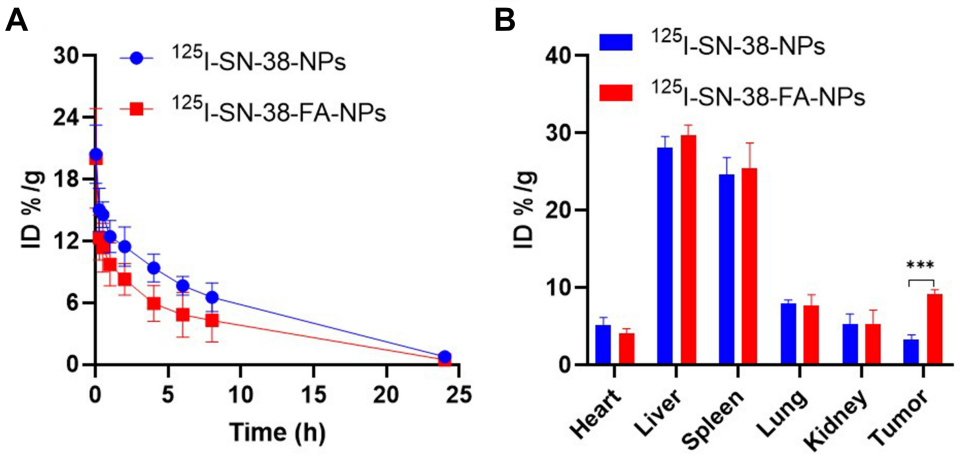

Figure 3 (**A**) Pharmacokinetics of ^{125}I-SN-38-NPs and ^{125}I-SN-38-FA-NPs (20 μCi) in healthy mice following intravenous injection (n=3). (**B**) Biodistribution of ^{125}I-SN-38-NPs and ^{125}I-SN-38-FA-NPs in MKN7 tumor-bearing mice after intravenous injection at 24 h (n=3). ***p < 0.001 were considered highly significant.

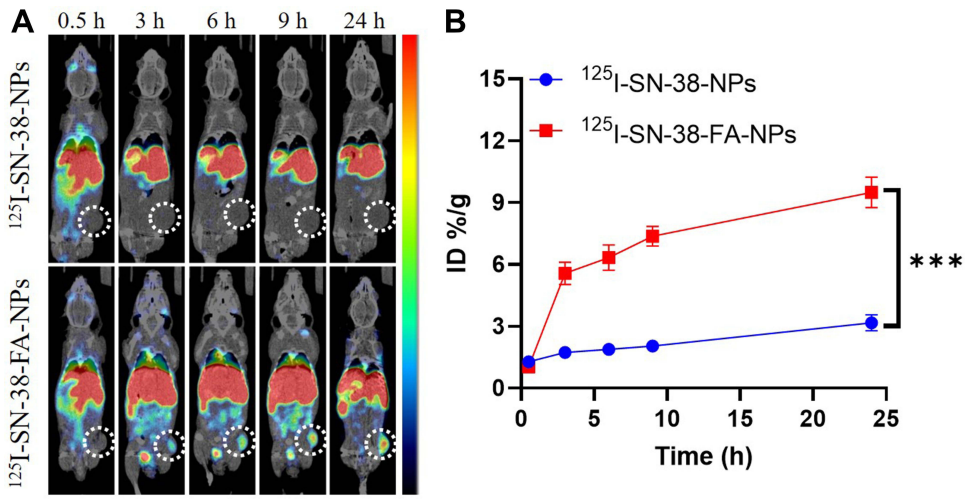

Figure 4 (**A**) *micro*SPECT/CT images of ^{125}I-SN-38-NPs and ^{125}I-SN-38-FA-NPs in MKN7 tumor-bearing mice following intravenous injection. (**B**) SPECT images of tumor uptake over time. ***$p < 0.001$ were considered highly significant.

(Figure 4A). The largest signals were detected in the liver and spleen, correlating with the biodistribution results. The radioactive signal of ^{125}I-SN-38-FA-NPs in tumors increased over time with the accumulation of ^{125}I-SN-38-FA-NPs rapidly increasing at 3 h postinjection, and reaching 9.2 ± 0.6%ID/g at 24 h postinjection. In contrast, the accumulation of ^{125}I-SN-38-NPs slowly increased to only 3.3 ± 0.6%ID/g at 24 h postinjection (Figure 4B), demonstrating that SN-38-FA-NPs exhibit highly efficient tumor accumulation in vivo.

In vivo Therapy Using Nanoparticles in MKN7 Tumor-Bearing Mice

MKN7 tumor-bearing mice were randomly divided into 5 treatment groups: PBS group, NP group, FA-NP group, SN-38-NP group, and SN-38-FA-NP group. PBS, NPs, FA-NPs, SN-38-NPs, and SN-38-FA-NPs were intravenously injected into mice via the tail vein with a dose of 100 mg/kg nanoparticles on Days 0, 5, 10, 15, and 20. Tumor volume was measured every 5 days by a Vernier caliper, and the mice body weights were examined. Tumors growth in the NP and FA-NP groups was comparable with the PBS group, indicating that they did not exhibit tumor inhibition. Tumor growth was slightly inhibited in the SN-38-NP group and significantly inhibited in the SN-38-FA-NP group. The tumor growth inhibition (TGI) was calculated according to the tumor volume. The TGIs of SN-38-FA-NPs and SN-38-NPs were 73% and 34%, respectively (Figure S3), demonstrating that SN-38-FA-NPs can effectively kill tumor cells (Figure 5A). After 20 days treatment and 20 days recovery, the mice were sacrificed, and tumors collected. Figure 5B shows a photo of the tumors in all 5 groups. No obvious body weight loss was found during the treatment (Figure 5C). TUNEL-stained images showed the SN-38-FA-NP group exhibited more apoptosis than the other groups (Figure 5D), no obvious damage to healthy organs was found in the H&E-stained images (Figure 6). These results demonstrate that SN-38-FA-NPs can effectively kill tumor cells without damaging healthy tissue, giving promise as a treatment for patients with gastric carcinoma.

Conclusion

In this study, we show that ^{125}I-radiolabelled SN-38 PLGA nanoparticles with folate surface modification are novel nanoplatforms for targeted gastric carcinoma theranostics. In vitro studies reveal the folate modification could enhance the uptake of nanoparticles in MKN7 cells. The quantification of *micro*SPECT images showed that ^{125}I-SN-38-FA-NPs had higher tumor accumulation than ^{125}I-SN-38-NPs at 24 h postinjection, and antitumor studies demonstrated that SN-38-FA-NPs effectively inhibit tumor growth without causing obvious side effect. ^{125}I-SN-38-FA-NPs also enable SPECT imaging and chemotherapy, providing a novel nanoplatform for gastric carcinoma theranostics.

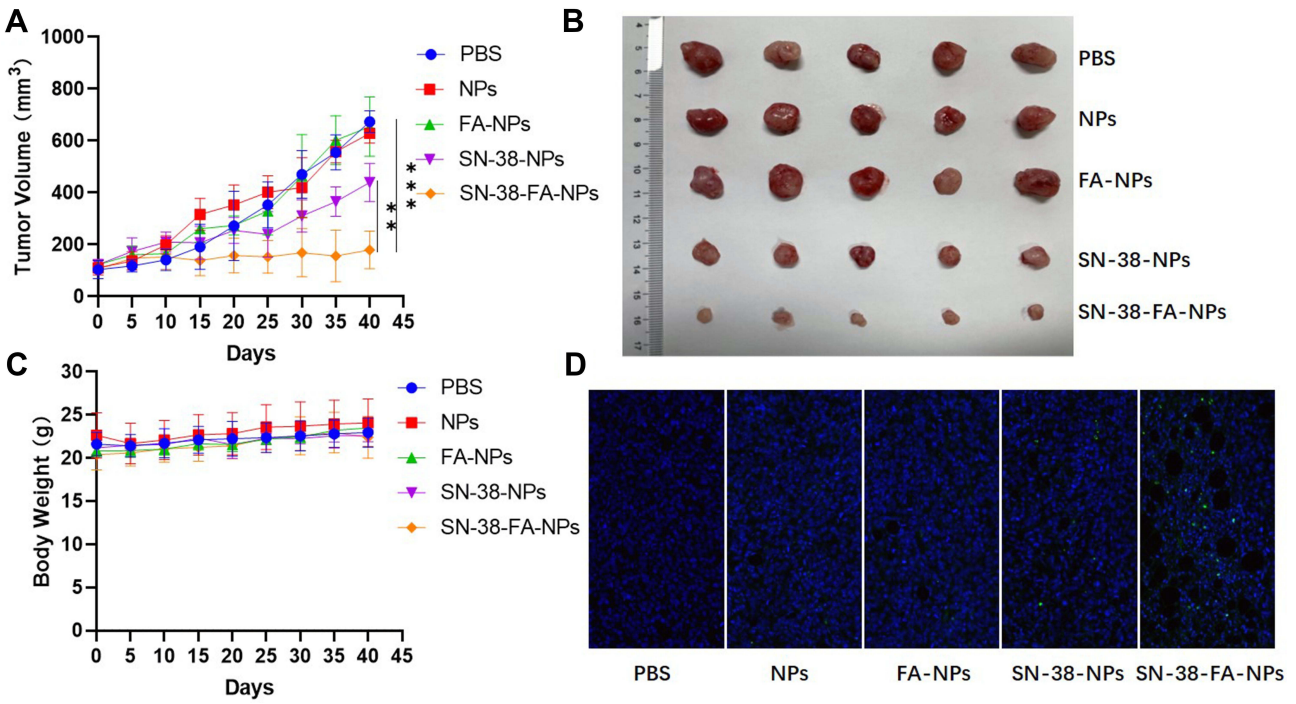

Figure 5 In vivo therapy. (**A**) Tumor growth rate. (**B**) Photograph of tumors after 40 days treatment. (**C**) Body weight changes in mice. (**D**) Microscopic images showing TUNNEL of tumors excised on Day 21. The scale bar corresponds to 50 μm. **p < 0.01 and ***p < 0.001 were considered highly significant.

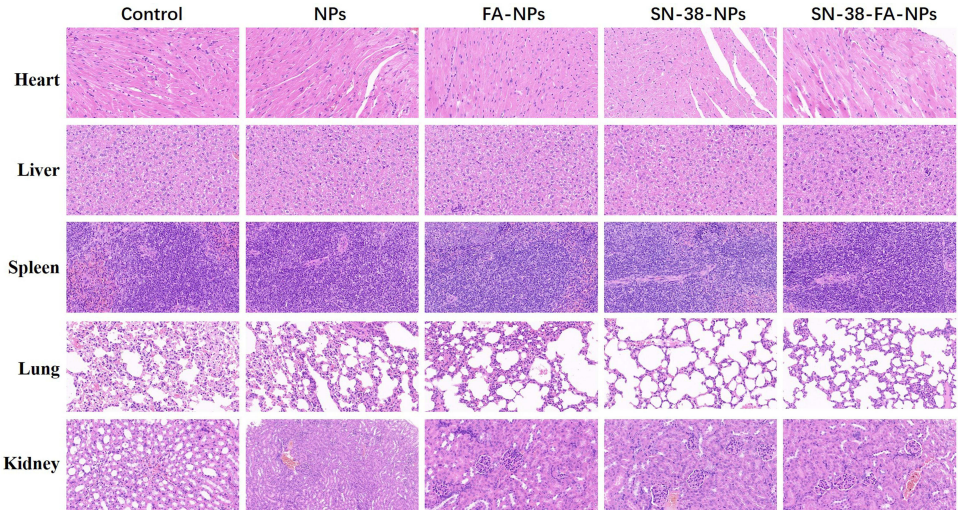

Figure 6 Microscopy images of H&E-stained major organs excised on Day 21. The scale bar corresponds to 50 μm.

Ethical Statement

All animal experiments were approved by the Animal Care and Use Committee of the Second Affiliated Hospital of the Naval Medical University, and all protocols using animals conformed to the Guide for the Care and Use of Laboratory Animals of the Second Affiliated Hospital of the Naval Medical University.

Acknowledgment

The authors thank the National Natural Science Foundation of China (81773049, 81402359, 81602617) for financial support.

Disclosure

The authors declare no competing financial/non financial interest.

References

1. Hoshi H. Management of gastric adenocarcinoma for general surgeons. *Surg Clin North Am*. 2020;100(3):523–534. doi:10.1016/j.suc.2020.02.004
2. Li Q, Xu X, Su D, Zhou T, Wang G, Li Z. Long-term survival of an elderly patient with advanced gastric cancer after combination therapy: a case report and literature review. *BMC Cancer*. 2019;19(1):459. doi:10.1186/s12885-019-5683-4
3. Davern M, Lysaght J. Cooperation between chemotherapy and immunotherapy in gastroesophageal cancers. *Cancer Lett*. 2020;495:89–99. doi:10.1016/j.canlet.2020.09.014
4. Al-Batran SE, Homann N, Pauligk C, et al. Perioperative chemotherapy with fluorouracil plus leucovorin, oxaliplatin, and docetaxel versus fluorouracil or capecitabine plus cisplatin and epirubicin for locally advanced, resectable gastric or gastro-oesophageal junction adenocarcinoma (FLOT4): a randomised, Phase 2/3 trial. *Lancet*. 2019;393(10184):1948–1957. doi:10.1016/S0140-6736(18)32557-1
5. Iyer R, Croucher JL, Chorny M, et al. Nanoparticle delivery of an SN38 conjugate is more effective than irinotecan in a mouse model of neuroblastoma. *Cancer Lett*. 2015;360(2):205–212. doi:10.1016/j.canlet.2015.02.011
6. Sharkey RM, McBride WJ, Cardillo TM, et al. Enhanced delivery of SN-38 to human tumor xenografts with an anti-trop-2-SN-38 antibody conjugate (Sacituzumab Govitecan). *Clin Cancer Res*. 2015;21(22):5131–5138. doi:10.1158/1078-0432.CCR-15-0670
7. Kawato Y, Aonuma M, Hirota Y, Kuga H, Sato K. Intracellular roles of SN-38, a metabolite of the camptothecin derivative CPT-11, in the antitumor effect of CPT-11. *Cancer Res*. 1991;51(16):4187–4191.
8. Huang Q, Wang L, Lu W. Evolution in medicinal chemistry of E-ring-modified Camptothecin analogs as anticancer agents. *Eur J Med Chem*. 2013;63:746–757. doi:10.1016/j.ejmech.2013.01.058
9. Roger E, Lagarce F, Benoit JP. Development and characterization of a novel lipid nanocapsule formulation of Sn38 for oral administration. *Eur J Pharm Biopharm*. 2011;79(1):181–188. doi:10.1016/j.ejpb.2011.01.021
10. Yang Z, Luo H, Cao Z, et al. Dual-targeting hybrid nanoparticles for the delivery of SN38 to Her2 and CD44 overexpressed human gastric cancer. *Nanoscale*. 2016;8(22):11543–11558. doi:10.1039/C6NR01749E
11. Palakurthi S. Challenges in SN38 drug delivery: current success and future directions. *Expert Opin Drug Deliv*. 2015;12(12):1911–1921. doi:10.1517/17425247.2015.1070142
12. Fang YP, Chuang CH, Wu YJ, Lin HC, Lu YC. SN38-loaded <100 nm targeted liposomes for improving poor solubility and minimizing burst release and toxicity: in vitro and in vivo study. *Int J Nanomedicine*. 2018;13:2789–2802. doi:10.2147/IJN.S158426
13. Indoria S, Singh V, Hsieh MF. Recent advances in theranostic polymeric nanoparticles for cancer treatment: a review. *Int J Pharm*. 2020;582:119314. doi:10.1016/j.ijpharm.2020.119314
14. Sah H, Thoma D, Desu S, Sah W, Wood T. Concepts and practices used to develop functional PLGA-based nanoparticulate systems. *Int J Nanomedicine*. 2013;8:747–765. doi:10.2147/IJN.S40579
15. Luo D, Carter KA, Razi A, et al. Doxorubicin encapsulated in stealth liposomes conferred with light-triggered drug release. *Biomaterials*. 2016;75:193–202. doi:10.1016/j.biomaterials.2015.10.027
16. Sadegh Malvajerd S, Azadi A, Izadi Z, et al. Brain delivery of curcumin using solid lipid nanoparticles and nanostructured lipid carriers: preparation, optimization, and pharmacokinetic evaluation. *ACS Chem Neurosci*. 2019;10(1):728–739. doi:10.1021/acschemneuro.8b00510
17. Hoshyar N, Gray S, Han H, Bao G. The effect of nanoparticle size on in vivo pharmacokinetics and cellular interaction. *Nanomedicine*. 2016;11(6):673–692. doi:10.2217/nnm.16.5
18. Turk MJ, Waters DJ, Low PS. Folate-conjugated liposomes preferentially target macrophages associated with ovarian carcinoma. *Cancer Lett*. 2004;213(2):165–172. doi:10.1016/j.canlet.2003.12.028
19. Parker N, Turk MJ, Westrick E, Lewis JD, Low PS, Leamon CP. Folate receptor expression in carcinomas and normal tissues determined by a quantitative radioligand binding assay. *Anal Biochem*. 2005;338(2):284–293. doi:10.1016/j.ab.2004.12.026
20. Zwicke GL, Mansoori GA, Jeffery CJ. Utilizing the folate receptor for active targeting of cancer nanotherapeutics. *Nano Rev*. 2012;3(1):18496. doi:10.3402/nano.v3i0.18496
21. Handali S, Moghimipour E, Kouchak M, et al. New folate receptor targeted nano liposomes for delivery of 5-fluorouracil to cancer cells: strong implication for enhanced potency and safety. *Life Sci*. 2019;227:39–50. doi:10.1016/j.lfs.2019.04.030
22. Marko AJ, Borah BM, Siters KE, et al. Targeted nanoparticles for fluorescence imaging of folate receptor positive tumors. *Biomolecules*. 2020;10(12):1651. doi:10.3390/biom10121651
23. Zhang DY, Zheng Y, Zhang H, et al. Folate receptor-targeted theranostic IrS(x) nanoparticles for multimodal imaging-guided combined chemo-photothermal therapy. *Nanoscale*. 2018;10(47):22252–22262. doi:10.1039/C8NR08095J
24. Farran B, Montenegro RC, Kasa P, et al. Folate-conjugated nanovehicles: strategies for cancer therapy. *Mater Sci Eng C Mater Biol Appl*. 2020;107:110341. doi:10.1016/j.msec.2019.110341
25. Werner ME, Copp JA, Karve S, et al. Folate-targeted polymeric nanoparticle formulation of docetaxel is an effective molecularly targeted radiosensitizer with efficacy dependent on the timing of radiotherapy. *ACS Nano*. 2011;5(11):8990–8998. doi:10.1021/nn203165z
26. Cao J, Wei Y, Zhang Y, Wang G, Ji X, Zhong Z. Iodine-rich polymersomes enable versatile SPECT/CT imaging and potent radioisotope therapy for tumor in vivo. *ACS Appl Mater Interfaces*. 2019;11(21):18953–18959. doi:10.1021/acsami.9b04294
27. Rogers W, Thulasi Seetha S, Refaee TAG, et al. Radiomics: from qualitative to quantitative imaging. *Br J Radiol*. 2020;93(1108):20190948. doi:10.1259/bjr.20190948
28. Pantel AR, Mankoff DA. Molecular imaging to guide systemic cancer therapy: illustrative examples of PET imaging cancer biomarkers. *Cancer Lett*. 2017;387:25–31. doi:10.1016/j.canlet.2016.05.008
29. Sirianni RW, Zheng MQ, Patel TR, et al. Radiolabeling of Poly(lactic- co -glycolic acid) (PLGA) nanoparticles with biotinylated F-18 prosthetic groups and imaging of their delivery to the brain with positron emission tomography. *Bioconjug Chem*. 2014;25(12):2157–2165. doi:10.1021/bc500315j

30. Barani M, Bilal M, Sabir F, Rahdar A, Kyzas GZ. Nanotechnology in ovarian cancer: diagnosis and treatment. *Life Sci*. 2021;266:118914. doi:10.1016/j.lfs.2020.118914
31. Vasiliu S, Racovita S, Gugoasa IA, Lungan MA, Popa M, Desbrieres J. The benefits of smart nanoparticles in dental applications. *Int J Mol Sci*. 2021;22(5):2585. doi:10.3390/ijms22052585
32. Jin Y, Wu Z, Li C, et al. Optimization of weight ratio for DSPE-PEG/TPGS hybrid micelles to improve drug retention and tumor penetration. *Pharm Res*. 2018;35(1):13. doi:10.1007/s11095-017-2340-y
33. Zhu Z, Wu M, Sun J, et al. Redox-sensitive iodinated polymersomes carrying histone deacetylase inhibitor as a dual-functional nano-radiosensitizer for enhanced radiotherapy of breast cancer. *Drug Deliv*. 2021;28(1):2301–2309. doi:10.1080/10717544.2021.1995080
34. Cardiff RD, Miller CH, Munn RJ. Manual hematoxylin and eosin staining of mouse tissue sections. *Cold Spring Harb Protoc*. 2014;2014(6):655–658. doi:10.1101/pdb.prot073411
35. Loo DT. In situ detection of apoptosis by the TUNEL assay: an overview of techniques. *Methods Mol Biol*. 2011;682:3–13.
36. Safa AR. Photoaffinity labeling of the multidrug-resistance-related P-glycoprotein with photoactive analogs of verapamil. *Proc Natl Acad Sci USA*. 1988;85(19):7187–7191. doi:10.1073/pnas.85.19.7187
37. Gupta E, Safa AR, Wang X, Ratain MJ. Pharmacokinetic modulation of irinotecan and metabolites by cyclosporin A. *Cancer Res*. 1996;56(6):1309–1314.
38. Yang X, Xue X, Luo Y, et al. Sub-100nm, long tumor retention SN-38-loaded photonic micelles for tri-modal cancer therapy. *J Control Release*. 2017;261:297–306. doi:10.1016/j.jconrel.2017.07.014
39. Wang DF, Rong WT, Lu Y, et al. TPGS 2k /PLGA nanoparticles for overcoming multidrug resistance by interfering mitochondria of human alveolar adenocarcinoma cells. *ACS Appl Mater Interfaces*. 2015;7(7):3888–3901. doi:10.1021/am508340m
40. Muniswamy VJ, Raval N, Gondaliya P, Tambe V, Kalia K, Tekade RK. "Dendrimer-Cationized-Albumin" encrusted polymeric nanoparticle improves BBB penetration and anticancer activity of doxorubicin. *Int J Pharm*. 2019;555:77–99. doi:10.1016/j.ijpharm.2018.11.035
41. Kim M, Pyo S, Kang CH, et al. Folate receptor 1 (FOLR1) targeted chimeric antigen receptor (CAR) T cells for the treatment of gastric cancer. *PLoS One*. 2018;13(6):e0198347. doi:10.1371/journal.pone.0198347
42. Shen X, Li T, Chen Z, et al. Luminescent/magnetic PLGA-based hybrid nanocomposites: a smart nanocarrier system for targeted codelivery and dual-modality imaging in cancer theranostics. *Int J Nanomedicine*. 2017;12:4299–4322. doi:10.2147/ijn.s136766
43. Operti MC, Bernhardt A, Grimm S, Engel A, Figdor CG, Tagit O. PLGA-based nanomedicines manufacturing: technologies overview and challenges in industrial scale-up. *Int J Pharm*. 2021;605:120807. doi:10.1016/j.ijpharm.2021.120807
44. Liu X, Wang J, Huang YW. Quantifying the effect of nano-TiO(2) on the toxicity of lead on C. dubia using a two-compartment modeling approach. *Chemosphere*. 2021;263:127958. doi:10.1016/j.chemosphere.2020.127958
45. Fang T, Zhu W, Li C, et al. Role of surface RGD patterns on protein nanocages in tumor targeting revealed using precise discrete models. *Small*. 2019;15(51):e1904838. doi:10.1002/smll.201904838
46. Atsumi R, Okazaki O, Hakusui H. Pharmacokinetics of SN-38 [(+)-(4S)-4,11-diethyl-4,9-dihydroxy-1H- pyrano[3',4':6,7]-indolizino[1,2-b]quinoline-3,14(4H,12H)-dione], an active metabolite of irinotecan, after a single intravenous dosing of 14C-SN-38 to rats. *Biol Pharm Bull*. 1995;18(8):1114–1119. doi:10.1248/bpb.18.1114
47. Kalyane D, Raval N, Maheshwari R, Tambe V, Kalia K, Tekade RK. Employment of enhanced permeability and retention effect (EPR): nanoparticle-based precision tools for targeting of therapeutic and diagnostic agent in cancer. *Mater Sci Eng C Mater Biol Appl*. 2019;98:1252–1276. doi:10.1016/j.msec.2019.01.066
48. Peng F, Setyawati MI, Tee JK, et al. Nanoparticles promote in vivo breast cancer cell intravasation and extravasation by inducing endothelial leakiness. *Nat Nanotechnol*. 2019;14(3):279–286. doi:10.1038/s41565-018-0356-z